INSTITUT DE FRANCE
Académie des sciences

Comptes Rendus

Chimie

Steffi Talwar, Alisha Shandil, Anoop Kumar Verma, Soumen Basu and Sunita Garhwal

Fe–TiO_2 composite beads driven hybrid process of photocatalysis and photo-Fenton for the degradation of isoproturon

Volume 23, issue 9-10 (2020), p. 533-549

Published online: 15 December 2020

https://doi.org/10.5802/crchim.52

This article is licensed under the
Creative Commons Attribution 4.0 International License.
http://creativecommons.org/licenses/by/4.0/

Les Comptes Rendus. Chimie *sont membres du*
Centre Mersenne pour l'édition scientifique ouverte
www.centre-mersenne.org
e-ISSN : 1878-1543

Comptes Rendus
Chimie
2020, 23, nº 9-10, p. 533-549
https://doi.org/10.5802/crchim.52

Full paper / *Mémoire*

Fe–TiO_2 composite beads driven hybrid process of photocatalysis and photo-Fenton for the degradation of isoproturon

Steffi Talwar [a], Alisha Shandil [b], Anoop Kumar Verma [*, c], Soumen Basu [d] and Sunita Garhwal [e]

[a] Research Scholar, Department of Chemical Engineering, Thapar Institute of Engineering and Technology, Patiala 147004, India

[b] Master of Science Student, School of Chemistry and Biochemistry, Thapar Institute of Engineering and Technology, Patiala 147004, India

[c] Associate Professor, School of Energy and Environment, Thapar Institute of Engineering and Technology, Patiala 147004, India

[d] Associate Professor, School of Chemistry and Biochemistry, Thapar Institute of Engineering and Technology, Patiala 147004, India

[e] Assistant Professor, Department of Computer Science and Engineering, Thapar Institute of Engineering and Technology, Patiala 147004, India

E-mails: steffi.talwar@gmail.com (S. Talwar), shandil.alisha95@gmail.com (A. Shandil), Anoop.kumar@thapar.edu (A. K. Verma), soumen.basu@thapar.edu (S. Basu), sgarhwal@thapar.edu (S. Garhwal)

Abstract. The concept of hybrid process of photo-Fenton and photocatalysis, particularly in the fixed mode, has been presented in this study for the degradation of the pesticide isoproturon with reduction at the time of treatment. For fixed-bed studies, spherical beads were prepared by combining definite proportions of clay, foundry sand, and fly ash, which were utilized as iron sources for titanium dioxide (TiO_2) immobilization. The optimization of various parameters was performed by utilizing the Box–Behnken design model under response surface methodology. The process of degradation followed first-order kinetics under an optimized condition for the integrated degradation of isoproturon with a 700 mg·L^{-1} dose of H_2O_2, 42 spherical beads, and 190 mL of solution for a duration of 176 min at pH 3.7. Approximately 80.96% degradation of isoproturon was observed after inducing the optimized conditions. The integrated treatment was also carried out in a solar batch reactor under optimized conditions to expand its application to industries for treating bio-recalcitrant compounds. The mineralization of isoproturon was confirmed through the generation of nitrate, nitrite, and ammonical nitrogen with a definite chemical oxygen demand reduction. The recyclability of the catalyst was confirmed by recycling the spherical beads characterized by scanning electron microscopy–energy dispersive X-Ray analysis. For confirming the dual effect, that is, the presence of TiO_2 along with Fe on the bead's surface, various analyses including UV–diffuse reflectance spectroscopy, scanning electron

* Corresponding author.

microscopy–energy-dispersive spectroscopy, X-ray diffraction, and Fourier-transform infrared spectroscopy were carried out. A tentative pathway for isoproturon removal was also predicted based on intermediate analysis through gas chromatography–mass spectroscopy.

Keywords. Isoproturon, Dual process, Composite beads, Fixed bed, Degradation.

Manuscript received 14th May 2020, revised 6th July 2020 and 20th October 2020, accepted 20th October 2020.

1. Introduction

The rapid growth in population with increased efforts on attaining sufficiency in food grains has pressurized Indian farmers to switch to the use of pesticides in considerable quantity. It has been estimated that predominantly for agricultural purposes, lakhs of tons of dichlorodiphenyltrichloroethane has been utilized in India alone due to its cost-effectiveness and excessive toxicity, making it effective in the control of pests [1]. However, certain features such as persistency, instability, and atmospheric distribution have led to the contamination of water, air, and soil [2]. Pesticides get washed away with water from fields and are drained off into rivers. This leads to a high toxic content in rivers. Hence, this causes pollution, which affects land and aquatic ecosystems in particular as the food for aquatic life becomes exposed to pesticides [3]. Pesticides enter the food chain, which affects our health. This has become a serious issue, which is certain to become more severe in the time to come.

Isoproturon 3-(4-isopropylphenyl)-1,1-dimethylurea is a selective herbicide that belongs to the family of substituted ureas. The herbicide is intended for use in cereals by controlling broadleaf weeds and annual grasses in them. The chemical is readily absorbed by the roots and leaves of weeds, thereby inhibiting photosynthesis. Various studies have confirmed the presence of isoproturon in fresh water due to production plant discharges, surface runoff, and runoff from agricultural sources [4].

More effective and efficient treatment techniques are required to reduce the environmental and potential effects of these pesticides containing effluents. Advanced oxidation processes (AOPs) are well cited in the literature to remove natural and inorganic toxins as well as for complete mineralization [5]. The AOP is an oxidative approach that involves the formation of a highly reactive intermediate radical (hydroxyl radical ($HO^{\bullet}$)) capable of oxidizing a large number of organic pollutants [6]. The $HO^{\bullet}$ can be produced through various techniques under the umbrella of AOPs, including photocatalysis, photo-Fenton, fixed-bed catalysis, and modified versions of these AOPs [7]. Although capable, they all pose certain operational drawbacks, which restrict their commercial-scale applications. The limitations of the Fenton process include the formation of iron sludge, which can be reduced by the application of ultraviolet irradiation or solar irradiation, the requirement of a high dose of hydrogen peroxide (H_2O_2), and the production of a large concentration of anions in the treated wastewater [8]. Certain pitfalls of photocatalysis include separation of the catalyst from the aqueous solution, thus generating an additional step in post-treatment. Recombination of electrons and holes is the other limitation that controls the rate of degradation [6]. Fixed-bed catalysis provides certain solutions for field-scale applications of AOPs. Studies related to the fixing of catalysts on supports are extensively cited in the literature [9]. Then again, some problems such as mass transfer limitations, inertness of supports, and time-consuming processes [10] pose impediments to field-scale applications.

Keeping in view the potential implications of all AOPs and field-scale applications, a hybrid process, called dual effect, has been studied, which can combine the pros and cons of the individual processes of photocatalysis and photo-Fenton [11]. The dual process prompts the generation of $HO^{\bullet}$ in large numbers because of the combined effects of photo-Fenton and titanium dioxide (TiO_2) photocatalysis. The basic mechanism involves the occurrence of photocatalysis on the surface and of the photo-Fenton in bulk [12–14]. It prevents the frequent recombination of electrons and holes by trapping the electrons from the conduction band for the production of Fe^{2+} ions, which are essential for the photo-Fenton reaction [15]. The investigation in this specific area of interest is always oriented toward reducing the time for treatment along with optimizing the process cost [16]. In the current study, the idea of incorporating the integrated effect (photo-Fenton and photocatalysis) was proposed to reduce

the treatment time of the isoproturon. The high dose of the chemicals used as well as the increased cost of the involved process can be reduced considerably if both the processes (photocatalysis and photo-Fenton) are run together, which would simultaneously increase the rate of degradation along with reducing the degradation time [17]. There are limited studies on the incorporation of dual processes for wastewater treatment. Therefore, the proposed study would maximize the photocatalytic efficiency of the system by including the dual effect (heterogeneous and homogeneous photocatalysis).

Hence, in the current study, the main focus is on the degradation of isoproturon using an in situ dual effect of photo-Fenton and photocatalysis. For the present study, composites were prepared by using the waste materials of industries as a source of iron. The prepared composite with a coating of TiO_2 enabled the dual effect to take place. The prepared support was also characterized using various techniques such as scanning electron microscopy–energy-dispersive spectroscopy (SEM–EDS), UV–diffuse reflectance spectroscopy (UV–DRS), and Fourier-transform infrared (FTIR) spectroscopy for the confirmation of TiO_2 along with the oxides of iron. For the optimization and the analysis of responses, the Box–Behnken design (BBD) was used. The process was intensified by varying parameters such as the number of beads, time, and the dose of H_2O_2.

2. Materials and methods

Isoproturon, a selective herbicide that belongs to the substituted urea family, is used for controlling the growth of annual grasses and weeds, specifically, wheat and barley. It is present in freshwater bodies at low concentrations due to its application in agricultural activities. Moreover, it is highly stable possessing low biodegradability. It was bought from Pioneer Pesticides Pvt. Ltd, Chandigarh (India) and was used as such without any further purification. TiO_2 P-25 was bought from Evonik (India). Clay, waste fly ash (FA), and foundry sand (FS) were collected as such from a nearby manufacturing unit (Patiala, India), and hydrogen peroxide (H_2O_2; 30% *w*/*v*), an oxidant, was acquired from Ranbaxy (India). For the preparation of acetate buffer for maintaining the pH, acetic acid (99.5% purity) and sodium acetate (98.5% purity) were procured from TCI Chemicals (India). For the preparation of all solutions, double distilled water was used.

Standard American Public Health Association (APHA) methods were followed for the monitoring and evaluation of nitrite [18], nitrate [19], and ammonium ions [20]. For estimating the concentrations of Fe(II) and Fe(III) leached from the beads under acidic conditions, the phenanthroline method was used according to APHA standards [21]. The chemical oxygen demand (COD) was estimated according to the closed reflux method and analyzed using a UV–Vis spectrophotometer (HACH, DR 5000, USA) [22]. The total organic carbon (TOC) content was monitored through a TOC analyzer (model Multi N/C 2100 BU, Analytic Jena AG Corporation, Germany). H_2O_2 interference was removed prior to COD and TOC determination by adding an adequate amount of concentrated solution of sodium carbonate followed by heating at 90 °C for 1 h as reported in the literature.

2.1. *Fabrication of the support material*

The materials used for preparing the composite beads were clay, FS, and FA. Bentonite and kaolin clay were used to provide binding to the composite beads. FS and FA have been proved to be a good blend of high-quality silica, aluminum oxides, iron oxides, calcium oxides, and some other oxides, which indicates their potential use in water/wastewater applications. The use of FA alone or FS alone does not provide the appropriate strength to the beads. Furthermore, clay alone does not yield the required amount of iron for the dual effect to take place.

Composite beads (spherical in shape) capable of introducing an integrated process of photo-Fenton and photocatalysis were prepared by mixing clay, FA, and FS in the ratio 2:1:1, respectively. These beads were calcined at 800 °C and were further immersed in water for 24 h to improve their strength. The average diameter of the bead was 25.5 mm as measured by taking its diameter from six to eight directions. The prepared composite was effectively coated with TiO_2 by immersing the composite completely in a TiO_2 slurry (2% *w*/*v*) using the standard dip coating technique [11]. The process of dip coating was performed twice for attaining the required thickness of the TiO_2 film on the composite. The beads were soaked for 48 h at a revolution speed of 10 rev/min.The average

thickness of the TiO_2 film was 65 μm with the average amount of TiO_2 on one bead being 1.6 mg.

2.2. *Experimental procedure for degradation*

For conducting the experiments, constant irradiation of a UV light source in a wooden chamber (36 W, seven tubes fitted at the top of chamber; UV-A, Philips) was carried out. A borosilicate glass reactor (8 cm × 2.6 cm) having a capacity of 500 mL was used for conducting the study (Figure S1, Supplementary Data). The initial concentration of isoproturon used for the degradation experiments was 25 mg·L^{-1}. The optimized number of catalyst-coated beads covering the whole surface was kept in the reactor in an adequate volume (200 mL) of isoproturon solution. The pH was maintained up to 3–3.5, and quantified H_2O_2 (750 mg·L^{-1}) was added. For the analysis of the results, at regular intervals of time, samples were withdrawn and analyzed using a Hitachi V-500 UV/VIS double-beam spectrophotometer at 239 nm. All the experiments were repeated thrice, and the mean of the results along with the standard deviation was reported (Table 2).

2.3. *Characterization techniques and analysis*

For depicting the morphology of the prepared composite, a scanning electron microscope (JSM-6510LV, JEOL, Japan) was used. The EDS assembly (INCAX-act, Oxford Instruments, UK) as an attachment to SEM was used for elemental analysis. An FTIR spectrometer was obtained from PerkinElmer (RX1) for the evaluation of the functional groups and linkages present in the prepared catalyst. UV–DRS (UV-2600, Shimadzu, Asia Pacific) was used for the evaluation of band gap energy. For the analysis of the organic transformation products of isoproturon, gas chromatography–mass spectroscopy (GC–MS) was carried out. A PerkinElmer Clarus 500 MS instrument was employed; its capillary columns were made of fused silica (25 m × 0.20 μm internal diameter) coated with 95% dimethyl polysiloxane/5% diphenyl. An injector temperature of 300 °C was used with the inlet line being set at 280 and 250 °C. Helium was used as the carrier gas, which had a flow rate of 1 mL/min at a run time of 30 min.

2.4. *Modeling and optimization*

Dual treatment of wastewater containing pesticides is quite complex as it involves the implementation of two different processes (photocatalysis and photo-Fenton) simultaneously. Hence, there are a large number of factors that would determine the rate of degradation of a particular compound such as mass transfer mechanisms, amount of $HO^{\bullet}$ formed, and various other limiting factors, which would be complex to understand. Modeling of dual treatment processes includes a multivariate system. It is obvious that this multivariate system cannot be solved by simple linear multivariate correlation [23]. It is also essential to study the interaction of parameters at a specific time. Hence, optimization was performed by utilizing response surface methodology (RSM) by varying different operational parameters to attain a suitable optimized condition. To optimize the process parameters, the BBD was employed [24].

The relationship between the input factors and responses is expressed as a quadratic response model. In general, the model used fits best in a polynomial equation of second order (1).

$$Y = s_0 + \sum_{i=1}^{k} s_i X_i + \sum^{k} s_{ii} X_i^2 + \sum \sum_{i<j} s_{ij} X_i X_j + \kappa_t, \quad (1)$$

where s_0, s_i, s_{ii}, and s_{ij} are constant coefficients, Y is the response, and X_i denotes independent variables. The Statistical Design-Expert software version 6.06 (STAT-EASE Inc., Minneapolis, USA) was used to design the experiments.

3. Results and discussion

3.1. *Characterization of the prepared composite used for the experiment*

The prepared composite beads, uncoated and TiO_2 coated, were analyzed using SEM. From Figure 1a, it is perceived that the surface of the composite is sufficiently rough for the coating to be stable and proper. Furthermore, the composition of the composite was proven by energy-dispersive X-ray spectrometry (EDS). The spectrum of the composite displays the signals of elements Fe, C, O, Al, Si, Ca, and Mg. The elements were present in the waste materials, and Al and Si were obtained from the clay used. The peaks of Fe confirmed that oxides of iron were

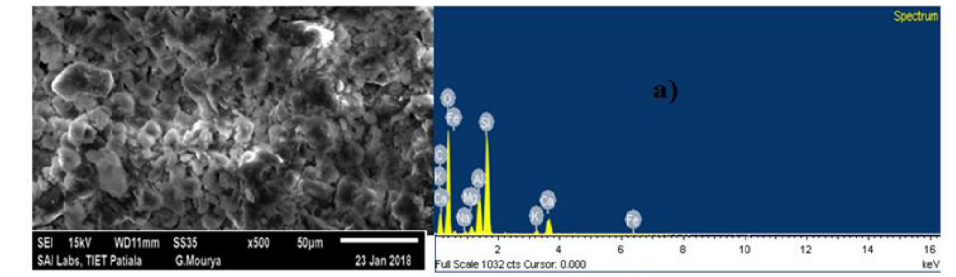

Elements	C K	Na K	Mg k	Al K	Si K	K K	Ca K	Fe K	O
Weight	11.26	0.56	1.16	5.62	15.05	1.47	5.56	2.89	56.44

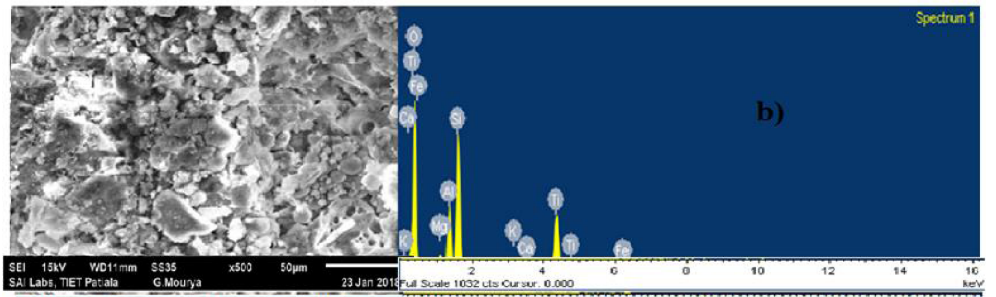

Elements	Ti K	Mg k	Al K	Si K	K K	Ca K	Fe K	O
Weight	23.35	1.44	6.98	17.89	1.66	1.08	2.88	44.73

Figure 1. (a) SEM–EDS of uncoated FA + FS spherical beads. (b) SEM–EDS of freshly TiO_2 coated FA + FS spherical beads.

present on the surface, thereby proving that the support was sufficiently suitable for the photo-Fenton reaction to take place. From Figure 1b TiO_2, the coating of fresh beads is evaluated. The TiO_2 coating was observed on the bead surfaces. The EDS analysis showed the occurrence of elements Ti, Fe, and O. This authenticates the presence of iron along with the coating of TiO_2, which enables the hybrid effect to take place. The concentration of iron present on the surface of composite beads was evaluated to be approximately 2.89 wt% from the EDS analysis.

The FTIR spectra for confirming the modifications with the prepared Fe–TiO_2 catalyst are shown in Figure 2. The analysis of the structure as well as the vibrations corresponding to the specific functional groups could be determined using FTIR spectroscopy. The peaks in the range 800–1200 cm^{-1} confirmed the presence of a Ti–O–Ti bond in the composite bead. The fingerprinting method could be applied for the analysis of the compounds present. Stretching vibrations related to the Si–O bond were also observed in the range of 550 cm^{-1}. The stretching vibrations of the O–H groups were related to the occurrence of transmittance bands at 3407.91 cm^{-1} and 3410.82 cm^{-1} in the case of TiO_2 and composite beads, respectively.

Owing to the increased activity of the prepared catalyst, the band gap energy was evaluated utilizing UV–Vis DRS. Basically, the reflectance of the sample and their light absorption capability were tested using UV–Vis DRS. A comparison was made between the band gap energy of P-25 TiO_2 alone and the freshly TiO_2 coated Fe composite (Figure 3). The scan was carried out ranging from 200 to 800 nm. There was a slight shift in the spectrum of the composite catalyst over TiO_2 alone, thereby indicating the capability of the composite catalyst to absorb light in the visible spectrum as shown in (2).

$$E = hc/\lambda, \tag{2}$$

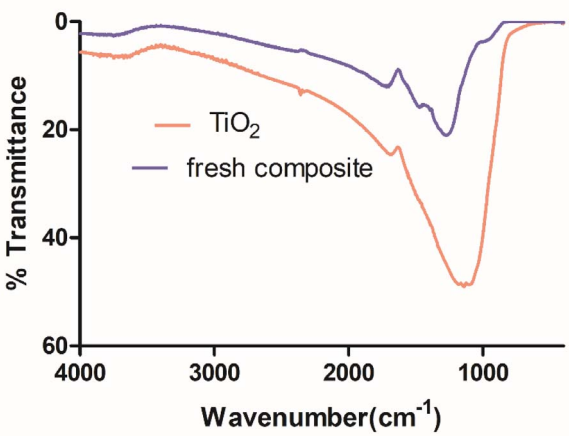

Figure 2. FTIR of TiO_2, fresh composite.

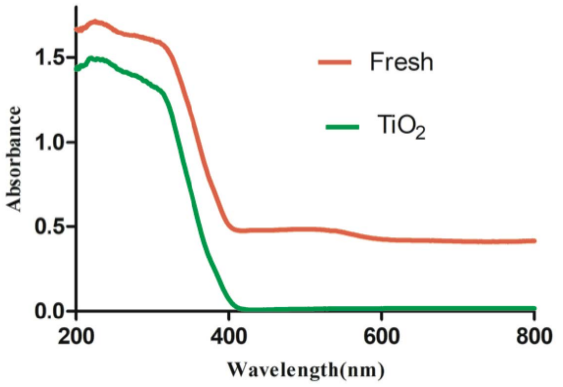

Figure 3. UV–Vis DRS of TiO_2 and the fresh composite.

where E is the band gap energy (eV), c is the speed of light (ms^{-1}), h is the Planck constant (4.135×10^{-6} eV), and λ is the wavelength (nm).

Accordingly, the value of the band gap energy was 3.2 eV for P-25 TiO_2 and 3.15 eV for the fresh catalyst (beads), confirming the activity of the catalyst even after the coating of catalyst on the composite beads.

For the crystalline phase analysis of the prepared composite, X-ray diffraction (XRD) analysis was carried out (Figure 4). Along with the presence of the anatase and rutile phases of TiO_2, the additional peaks corresponding to the oxides of iron with titanium were also observed. The occurrence of the dual effect, that is, photocatalysis and photo-Fenton taking place simultaneously, has been also proven.

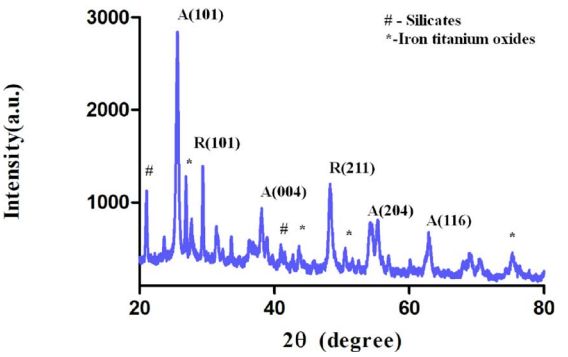

Figure 4. XRD analysis of the freshly coated composite.

3.2. *Performance analysis of the prepared composite*

For the application of the prepared composite of Fe and TiO_2, isoproturon was used as the model compound. The catalyst exhibits the inherent properties of Fe^{2+} and Fe^{3+}, indicating their presence as well as a layer of TiO_2. This enables both photocatalysis and photo-Fenton reactions to take place simultaneously.

For proving the ability of the prepared catalyst, various preliminary experiments including adsorption, photolysis, UV + H_2O_2, photocatalysis, photo-Fenton, and combined photocatalysis and photo-Fenton (i.e., dual process) were performed (Figure 5a). For conducting the photo-Fenton experiments, 40 uncoated beads covering the whole surface were kept in a reactor at an adequate volume (200 mL). The pH was maintained up to 3–3.5, and quantified H_2O_2 (750 $mg{\cdot}L^{-1}$) was added. For the photocatalysis process, TiO_2 coated beads were used under the same conditions as those for photo-Fenton. For adsorption, TiO_2 coated beads were used after adding the beads to an isoproturon solution. The reactor was placed in the dark. Even after 180 min, only $2.05 \pm 1\%$ of isoproturon adsorption was observed, whereas photolysis contributed to a reduction of $11.25 \pm 2.5\%$ in isoproturon concentration after 180 min. Photocatalysis resulted in a reasonable degradation of isoproturon, $57.7 \pm 5\%$ in 180 min, as compared to photo-Fenton, which led to a reduction of $29.9 \pm 5\%$ in the concentration of the compound at the same time. However, the combined effect of both photocatalysis and photo-Fenton (Fe + UV + TiO_2 + H_2O_2) produced the best

Table 1. Variation in variables and coded levels

Factor	Name	Low actual	High actual	Low coded	High coded
A	Variation in H_2O_2 ($mg{\cdot}L^{-1}$)	375	1125	−1	1
B	Number of beads	30	90	−1	1
C	Volume of solution (ml)	150	400	1	1
D	Time	30.00	180	1	1

results as a degradation of 80.96% was observed under the same conditions. This reveals that the occurrence of Fe with TiO_2 leads to the acceleration of the reaction in the presence of H_2O_2. For practical real-life applications, this study can be a base on which further parameters can be optimized according to scale-up calculations. For validating the technology in real-life applications, authors have published few papers on real industry effluents [25]. The lower pH of the wastewater enabled the photo-Fenton reactions to take place. For practical and economic purposes, low-pH water could be procured from acid industries, which face the problem of disposing low-pH wastewater.

For further optimization of the degradation process, various parameters such as the number of beads, H_2O_2 dose, volume of the solution (wastewater), and degradation time were utilized. Table 1 presents the various optimum conditions and their maximum and minimum limits. Overall, 29 experiments were suggested by the BBD for optimizing the process parameters such as the H_2O_2 dose from 375 to 1125 $mg{\cdot}L^{-1}$, the number of beads from 30 to 90 in the 500 mL batch reactor depending on the exposed area of the reactor (i.e., 30 beads covering approximately 50%, 60 beads covering approximately 100%, and 90 beads covering 150% of the reactor surface area), the volume of the solution ranging from 150 to 400 ml (wastewater), and the degradation time from 30 to 180 min for isoproturon as shown in Table 2.

H_2O_2 plays a dual role in the proposed hybrid process of photo-Fenton as well as photocatalysis. It is consumed simultaneously in both the processes, leading to enhanced production of $HO^{\bullet}$. H_2O_2 along with ferrous ions (leached from composite beads) leads to the formation of $HO^{\bullet}$ (i.e., photo-Fenton); see Figure 5b). The H_2O_2 reacts with the superoxide radicals formed in the photocatalysis, leading to additional production of $HO^{\bullet}$. The in situ H_2O_2 photolysis also adds to the $HO^{\bullet}$ pool. Hence, $HO^{\bullet}$ produced in abundance leads to an increased rate of degradation. In the dual as well as the individual processes of photocatalysis and photo-Fenton, H_2O_2 plays a very important role. The decomposition of H_2O_2 has been studied on the surface of various catalysts such as Fe, TiO_2, CuO, and many more [26]. It was observed that in the dark, there was negligible change in the concentration of H_2O_2. However, here there was significant change in the concentration, that is, the decline in H_2O_2 concentration was observed in the dual process. This confirms the role of the dual process in the decomposition of H_2O_2 (Figure S2). A high consumption of H_2O_2 was observed in the case of the dual process. Thus, it was concluded that in the presence of light, along with TiO_2 and iron, the decomposition of H_2O_2 is accelerated with greater production of •OH.

The three-dimensional (3D) response graph plotted against H_2O_2 dose and number of beads for the degradation of isoproturon is depicted in Figure 6(a). The graph was plotted for an optimized time of 175 min. H_2O_2 was not completely used after the reactions. With increase in H_2O_2 concentration from 375 $mg{\cdot}L^{-1}$ to 750 $mg{\cdot}L^{-1}$, there is a slight increase in percentage degradation due to the production of an increased amount of HO radicals. On further increasing the concentration to 1125 $mg{\cdot}L^{-1}$, the degradation rate of isoproturon decreases, which may be attributed to the scavenging effect of H_2O_2. This involves the formation of excess $HO_2^{\bullet}$ radicals when $HO^{\bullet}$ radicals combine with H_2O_2 as expressed in (3):

$$\bullet OH + H_2O_2 \rightarrow HO_2^{\bullet} + H_2O \quad (3)$$

Maximizing the utilization rate of H_2O_2 and minimizing the utilized amount of H_2O_2 is conducive to its industrial application.

Figure 6a shows that with increase in the number of beads from 30 to 60, the percentage degradation of isoproturon would undergo an increment. However, with further increase in the number of beads, there is

Table 2. Full factorial BBD matrix with standard deviation

Sl. No.	Variation in H_2O_2 ($mg{\cdot}L^{-1}$)	Number of beads	Volume of solution (mL)	Time (min)	% degradation (standard deviation calculated from triplicates; same beads were used)
1	750	90	400	105	44.64 ± 2.573
2	750	30	275	30	20.34 ± 0.466
3	750	60	400	180	63.57 ± 1.110
4	375	60	150	105	60.09 ± 1.350
5	1125	90	275	105	21.56 ± 0.311
6	750	90	275	180	68.21 ± 1.562
7	1125	60	400	105	28.41 ± 1.704
8	1125	60	275	30	10.24 ± 0.537
9	750	30	275	180	68.05 ± 1.449
10	1125	60	275	180	79.12 ± 0.622
11	750	60	275	105	44.87 ± 0.091
12	1125	30	275	105	23.93 ± 1.463
13	750	90	150	105	15.49 ± 0.360
14	375	90	275	105	40.53 ± 1.039
15	375	60	400	105	41.53 ± 1.746
16	750	60	275	105	52.11 ± 1.491
17	375	30	275	105	44.87 ± 0.091
18	750	30	150	105	60.25 ± 1.237
19	750	60	150	30	24.19 ± 1.548
20	750	60	275	105	56.44 ± 1.018
21	750	60	275	105	50.44 ± 1.103
22	750	60	400	30	5.06 ± 0.749
23	750	30	400	105	27.53 ± 0.332
24	375	60	275	30	24.14 ± 0.806
25	1125	60	150	105	26.35 ± 0.954
26	750	90	275	30	18.97 ± 0.685
27	375	60	275	180	70.11 ± 0.629
28	750	60	275	105	48.99 ± 1.407
29	750	60	150	180	78.33 ± 0.940

a decrease in percentage degradation. As discussed, the number of beads was varied as per the available surface area of the reactor. In fact, more number of beads would eventually lead to an increase in the concentration of iron in the solution, which would hinder the reaction due to the blockage of active sites. Moreover, an excess number of beads would trap the solution in the void, thus leading to dead zones.

The 3D response graph plotted against H_2O_2 dose and volume of the solution for the percentage degradation of isoproturon is depicted in Figure 6b. The number of beads as shown in Figure 6b is 42. This indicates that with increase in volume of the solution from 150 mL to 275 mL, there is negligible effect on the percentage degradation. Moreover, with further increase in volume, the percentage degradation decreases considerably due to ineffective penetration of UV radiation as the volume of the solution ultimately causes lesser degradation. On the other hand, the change in the concentration of H_2O_2 from

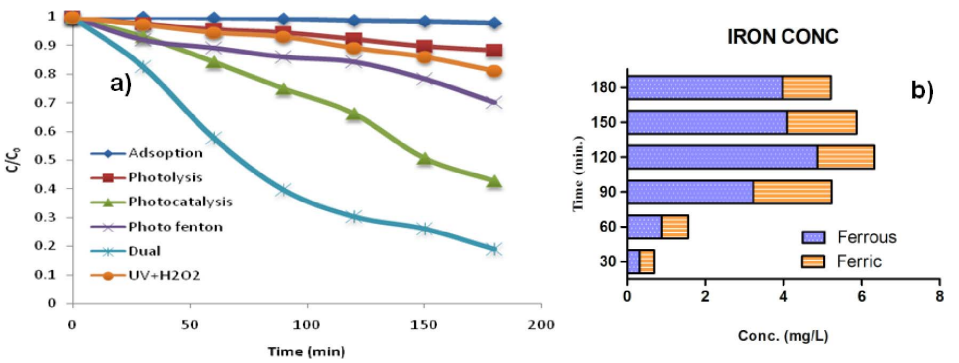

Figure 5. Outcomes of different preliminary reactions to assess the advantage and effectiveness of each condition.

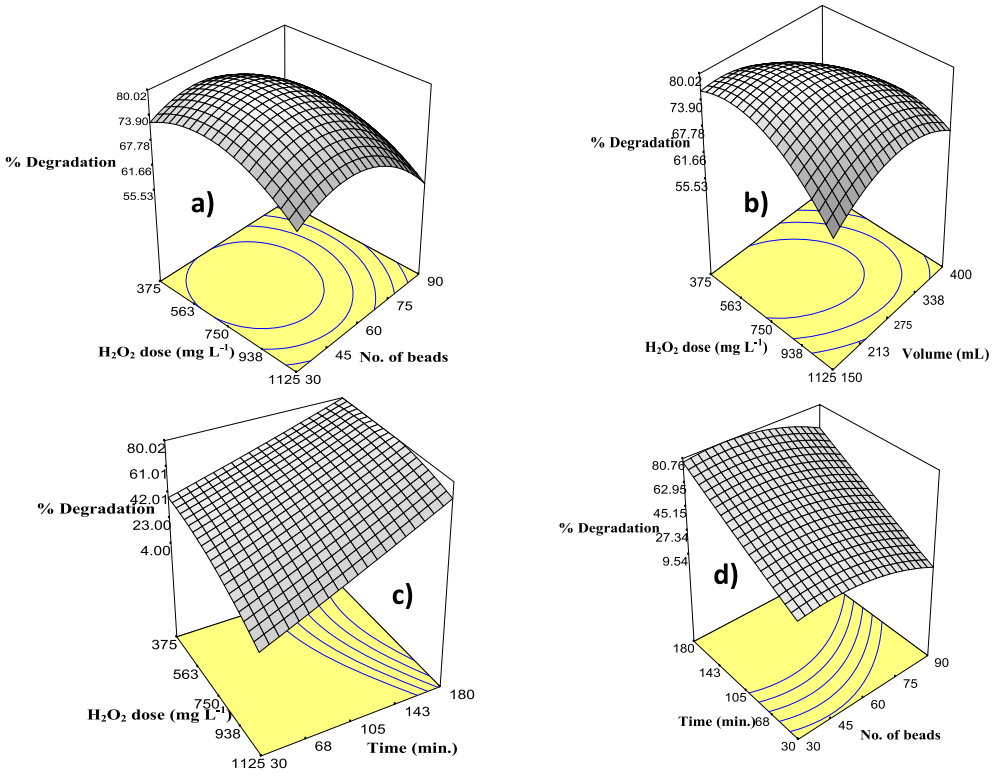

Figure 6. (a) 3D response surface graph for percentage degradation of isoproturon by variation in H_2O_2 dose and number of beads. (b) 3D response surface graph for percentage degradation of isoproturon by variation in H_2O_2 dose and volume of wastewater. (c) 3D response surface graph for percentage degradation of isoproturon by variation in H_2O_2 dose and time. (d) 3D response surface graph for percentage degradation of isoproturon by variation in time and number of beads.

375 mg·L^{-1} to 750 mg·L^{-1} causes a slight increase in percentage degradation, which eventually would decrease with further increase in concentration to 1125 mg·L^{-1} due to the scavenging effect expressed in (3). As we implement a dual process, the amount of H_2O_2 is used in both the processes simultaneously,

Table 3. Sequential model sum of squares

Source	Sum of squares	Degree of freedom	Mean square	F-value	Prob > F	
Mean	51177.00	1	51177.00			
Linear	9820.31	4	2455.08	21.75	<0.0001	
2FI	1200.81	6	200.13	2.39	0.07	
Quadratic	848.82	4	212.21	4.51	0.01	Suggested
Cubic	513.70	8	64.21	2.65	0.12	Aliased
Residual	145.41	6	24.23			
Total	63706.05	29	2196.76			

that is, in photocatalysis as well as in photo-Fenton. At low concentrations of H_2O_2, the process takes place at a slow pace as this compound is utilized in both the reactions. The optimized dose of H_2O_2 used was 700 mg·L^{-1}.

An analysis of the 3D response graph plotted against H_2O_2 dose and time for the percentage degradation of isoproturon shows that there is a sharp increase in percentage degradation with increment in time as depicted in Figure 6c. Clearly, with more exposure time experienced by the solution under UV light, there is enhanced production of HO$^{\bullet}$. The variation in H_2O_2 dose causes a scavenging effect with increase in volume. From Figure 6d (H_2O_2 700 mg·L^{-1}), it is observed that when the number of beads is increased up to 45 at the maximum time, the degradation of isoproturon increases, which remains almost constant up to 60 beads. This is basically due to the increase in the dose of the catalyst (i.e., both TiO_2 and the iron content), leading to the process occurring at a faster pace. There is almost 80% degradation when the number of beads is 60, hence ideally covering 100% area of the reactor.

The optimum conditions for the dual treatment of isoproturon were verified experimentally. The experiment was run for 176 min at pH 3.7 with 42 beads, 190 mL of wastewater, and 700 mg·L^{-1} of H_2O_2 dose. At this optimum condition, the percentage degradation of isoproturon at a concentration of 25 ppm was estimated to be 80.96%. The model confirmed effective degradation of the contaminant.

3.3. *Statistical analysis*

For the selection of the best model, a sequence of F-test and other required measures was used. The p-value for the degradation of isoproturon was found to be less than 0.01 for the quadratic model evaluated by the sequential model sum of squares [27]. As regards the model summary statistics and the sequential model sum of squares, the adequacy of the model was tested. The result of the adequacy of the model is shown in Table 3 for the percentage degradation of isoproturon. For the percentage degradation of isoproturon, the quadratic model showed the perfect fit using the sequential model sum of squares.

For the quadratic model, the Prob > F-value was 0.0151, suggesting it to be significant. For the quadratic model, the coefficient of determination was 0.94. This indicates a good correlation between the predicted and observed values. The predicted values were quite close to the actual values. The difference between the predicted values and observed values divided by the standard error of the residual has a close relationship with the percentage normal probability.

The analysis of variance (ANOVA) indicates that the F-value for the percentage degradation of isoproturon is 18.01 as shown in Table 4. The significance of the model is revealed by the F-value of 18.01. The chances for the occurrence of a large F-value are only 0.01%, which might be due to noise. The "Prob > F-values" larger than 0.100 indicate that the model is insignificant.

From the ANOVA, it is clear that the variation in H_2O_2, volume of solution, time, (variation in H_2O_2)^2, (number of beads)^2, (volume of solution)^2, and interaction between the number of beads and the volume of solution are highly significant for the percentage degradation of isoproturon.

The second-order quadratic equation obtained in terms of significant interaction parameters and

Table 4. The ANOVA suggested by BBD for the percentage degradation of isoproturon

Source		Sum of squares	Degree of freedom	Mean square	F-value	Prob > F	
	Model	11869.94	14	847.85	18.01	<0.0001	Significant
	Variation in H_2O_2	699.98	1	699.98	14.87	0.0017	
	Number of beads	105.38	1	105.38	2.24	0.15	
	Volume of solution	242.64	1	242.64	5.15	0.039	
	Time	8772.32	1	8772.32	186.33	<0.0001	Highly significant
	(Variation in H_2O_2)^2	286.45	1	286.45	6.08	0.027	
	(Number of beads)^2	492.00	1	492.00	10.45	0.006	
	(Volume of solution)^2	239.32	1	239.32	5.08	0.040	
	(Time)^2	4.02	1	4.02	0.085	0.77	
	Variation in H_2O_2 × Number of beads	0.96	1	0.96	0.020	0.88	
	Variation in H_2O_2 × Volume of solution	106.30	1	106.30	2.26	0.15	
	Variation in H_2O_2 × Time	131.22	1	131.22	2.79	0.11	
	Number of beads × Volume of solution	956.97	1	956.97	20.33	0.0005	
	Number of beads × Time	0.59	1	0.59	0.012	0.91	
	Volume of solution × Time	4.77	1	4.77	0.10	0.75	
Residual		659.11	14	47.08			
Lack of fit		587.24	10	58.72	3.27	0.13	Not significant
Pure error		71.87	4	17.97			
Corrected total sum of squares		12529.05	28				

process parameters is presented in (4):

$$\begin{aligned}\text{Degradation} = {} & 67.68 - (5.58 \times \text{H}_2\text{O}_2 \text{ variation}) \\ & - (0.16 \times \text{volume}) + (0.13 \times \text{time}) \\ & - (106.32 \times \text{H}_2\text{O}_2 \text{ variation}^2) \\ & - (9.67 \times 10^{-3} \times \text{ no. of beads}^2) \\ & - (3.88 \times 10^{-4} \times \text{volume}^2) \\ & + \left(4.12 \times 10^{-3} \times \text{ no. of beads} \times \text{volume}\right). \end{aligned} \tag{4}$$

3.4. *Kinetic study and synergistic calculations*

Pseudo-first-order kinetics were used for the evaluation of the rate equations of the dual process as presented in (5)–(9):

$$\text{Rate} = -\frac{\text{d}(I)}{\text{d}t} = k(I), \tag{5}$$

$$\frac{\text{d}(I)}{(I)} = -k\,\text{d}t, \tag{6}$$

$$\int_{(I_0)}^{(I)} \frac{\text{d}(I)}{(I)} = \int -k\,\text{d}t, \tag{7}$$

$$\ln(I) - \ln(I_0) = -kt, \tag{8}$$

$$\ln\frac{(I)}{(I_0)} = -kt, \tag{9}$$

where the concentrations of the isoproturon (in mg·L^{-1}) are denoted by I, I_0 (initial), I (at any time t in minutes); the time for the degradation of isoproturon is denoted by t; the rate constant following the pseudo-first-order is denoted by k (in min^{-1}). The

value of the slope (k) can be determined by the natural logarithm of $(I)/(I_0)$ and the time required for degradation. For the dual process, the k value was significantly higher (i.e., 0.009 min^{-1}), whereas the rate constants for photocatalysis and photo-Fenton were 0.004 and 0.001 min^{-1}, respectively.

Synergy is the term used to represent the efficacy of the improved process over the conventional processes. The rate constants calculated from the kinetics data are used to quantify the synergy [28]. The synergy is calculated using (10):

$$\begin{gathered}\text{Synergy} = \frac{(k)_{\text{dual}}}{(k)_{\text{photocatalysis}} + (k)_{\text{photo-Fenton}}},\\ \text{Synergy} = \frac{0.009}{0.001 + 0.004},\\ \text{Synergy} = 1.8.\end{gathered} \tag{10}$$

The results confirmed that there was a huge increase in synergy when using both the processes at the same place and at the same time other than when using individual processes. The rate constant is calculated for the complete process. It is not calculated for only end of reaction, but is the conjunction of the complete reaction. the complete reaction. A synergy index equal to 1 indicates identical isoproturon degradation properties of the combined and the sum of the individual systems, whereas a synergy index >1 exhibits an improved degradation of the combined system.

3.5. *Scale-up studies*

To visualize the field-scale applications, a scale-up experiment was performed in sunlight using a baffled glass reactor with dimensions (25 cm × 30 cm × 5 cm) designed to handle the total volume of 5 L. TiO_2 immobilized composite beads were used to conduct in situ dual effect experiments. The synthetic wastewater from the pesticide, under acidic conditions, containing an optimized dose of H_2O_2 was pumped from a collection tank with the help of a pump. The flow rate was maintained at 2.5 $L{\cdot}h^{-1}$ (Figure 7a). The intensity was measured using a pyranometer (MP-100, Apogee) and was averaged to 920 $W{\cdot}m^{-2}$ for that period. From Figure 7b, it was observed that for 180 min initially, the degradation rate was fast. The rate increased to 71%, which might be basically due to the predominance of photocatalysis, that is, the presence of a TiO_2 layer as well as Fe leaching, leading to homogeneous photocatalysis, as fresh beads come in contact with the effluent, resulting in faster degradation. With further increase in treatment time, there was a slight increase in the rate of degradation, that is, approximately 78% of degradation was observed after 250 min. The degradation rate remained mostly constant after this, which might be due to the stabilization of various products formed by the conversion of isoproturon. This study ensures the commercial-scale viability of the process.

Table 5. Estimated value of E_{EO} for degradation processes

Degradation processes	Energy consumption (E_{EO}) ($MW{\cdot}h{\cdot}m^{-3}$)
Photo-Fenton	25.30
Photocatalysis	10.39
Dual effect	5.28

3.6. *Energy consumption*

A comparison can be drawn by measuring the consumption of energy (E_{EO}) for the integrated effect on the percentage degradation of isoproturon and energy consumption in the case of individual processes of photo-Fenton and photocatalysis. E_{EO} can be described as the requirement of electrical energy for the degradation of contaminant concentration (m^3) of the wastewater. The value of E_{EO} ($kW{\cdot}h{\cdot}m^{-3}{\cdot}order^{-1}$) can be calculated by utilizing (11):

$$E_{E0} = \frac{P \times t \times 1000}{V \times 60 \times \log\left(\frac{I_i}{I_f}\right)}. \tag{11}$$

In this equation, the power consumed by the UV lamps (kW) is denoted by P, V is the volume (L) of the water in the reactor, I_i and I_f are the initial and final concentrations ($mg{\cdot}L^{-1}$) of isoproturon, and t is the irradiation time (min).

It can be observed that the E_{EO} value was comparatively very less in the case of dual effect (Table 5) due to the intactness of TiO_2 activity and simultaneous photo-Fenton owing to iron content leaching from the beads causing effective degradation.

3.7. *Durability studies*

The durability studies of supported catalysts are very important in the case of fixed-bed catalysis. These

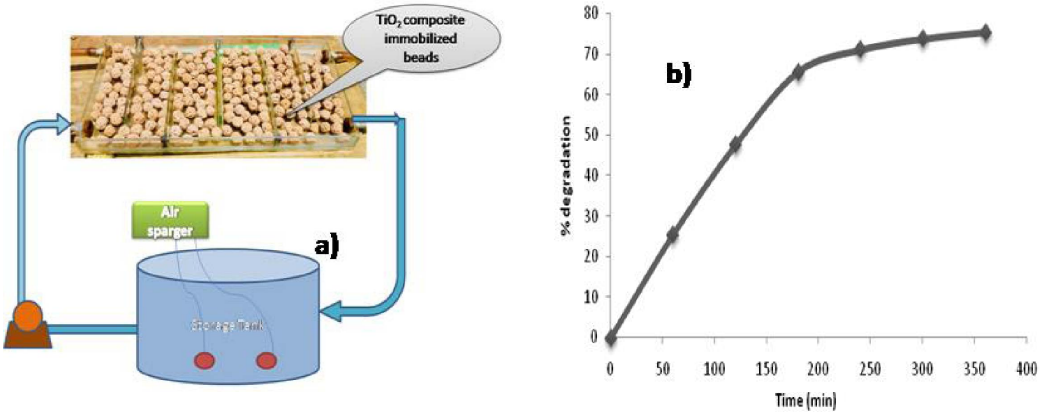

Figure 7. (a) Image of fixed-bed reactor scale-up (V = 5 L). (b) Time vs. percentage degradation of isoproturon using fixed-bed reactor scale-up.

studies are even more complex in our reported dual process of photocatalysis and photo-Fenton. In fact, the process has to maintain the activity of coated TiO_2 along with sustaining iron leaching. The activity of a catalyst decreases with every cycle, but it can be reactivated at high temperatures. However, this is not economically feasible [25]. We have made efforts to study the durability of TiO_2 coated (clay + FS + FA) beads used for the degradation of isoproturon in wastewater. The same beads were used to prove the recyclability/durability of the composite. The durability was maintained in dual effect. That is, there was stable coating of TiO_2 even after many recycling steps and subsequent leaching of iron with the recycling. Hence, the beads were adequately recycled for at least 40 to 50 times without any effective decrease in efficiency with respect to the percentage degradation of isoproturon as shown in Figure 8a. There was not much change in the iron concentration even after 35 recycling steps (Figure 8b). After every cycle, the beads were reactivated by placing them in a heating oven at 100 °C for a duration of 1 h. A small amount of reduction in the photocatalytic activity is due to the loss of TiO_2 coating with every cycle. The gradual reduction in dual effect (10–12%) after 30 cycles may be attributed to the loss of the catalyst and less amount of iron leaching into the solution during consecutive cycles of the reaction. The stability of the catalyst and the presence of iron in the beads were determined by SEM–EDS of the fresh beads, coated beads, and recycled immobilized beads. It was found that the catalyst was intact and iron was still actively leaching even after 35 cycles.

3.8. *Characterization of recycled beads*

The SEM–EDS image of the recycled beads (40 cycles) shows the presence of TiO_2 on the bead surface with a little loss of TiO_2 coating after repeated cycles (Figure 9a). The presence of Fe, Ti, and O was confirmed by the appearance of distinct peaks in EDS.

The evaluation of the band gap energy by UV–Vis DRS of the recycled-catalyst-coated Fe composite yielded an energy of 3.10 eV for the recycled catalyst (beads), confirming the activity of the catalyst even after repeated use (Figure 9b).

The recycled composite was further evaluated using FTIR (Figure 10a). The graph followed the same pattern as that of the unused composite beads. The scan depicts the appearance of peaks in the range 800–1200 cm^{-1} for both the fresh and recycled spectra, verifying the presence of Ti–O–Ti bonds in both the samples. This proves the retention of TiO_2 lattices in the case of immobilized beads. In the initial few cycles, TiO_2 weathering off from the support. At the same time, the coating may not be uniform for all the beads. Furthermore, there are fewer dense pockets of TiO_2 at some scattered locations on the beads.

For the structural analysis of the recycled catalyst, XRD analysis was carried out (Figure 10b). Along with the peaks indicating the basic characteristics of TiO_2 (i.e., anatase and rutile phases), the peaks of

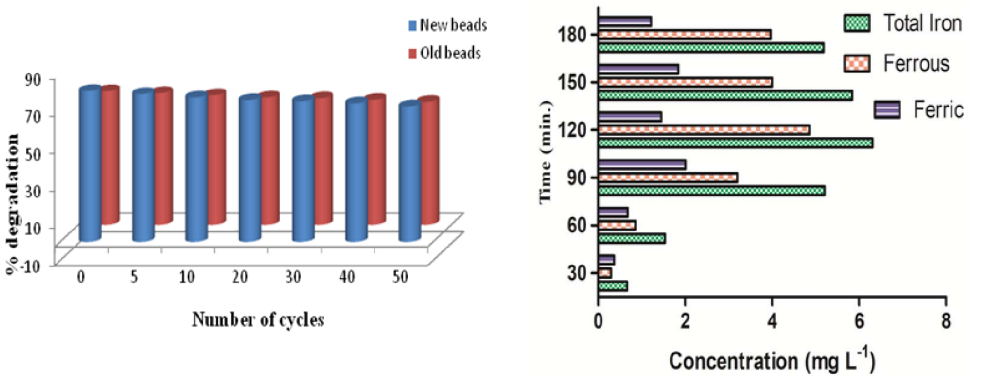

Figure 8. (a) Durability studies of fresh and recycled beads for percentage degradation of isoproturon using dual effect. (b) Estimation of the iron content in terms of ferrous and ferric content after recycling.

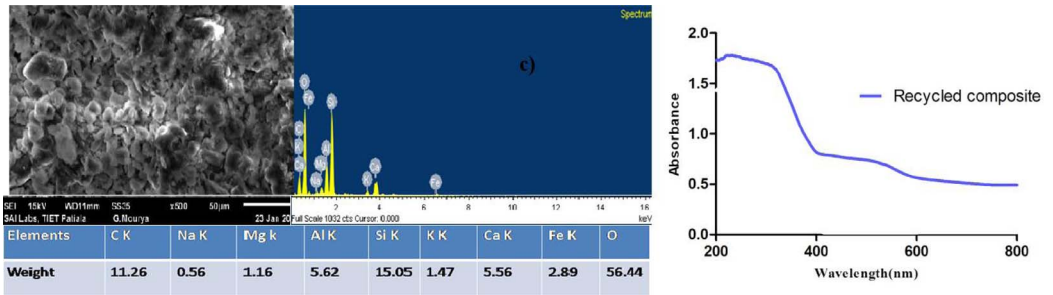

Figure 9. (a) SEM–EDS of recycled TiO_2 coated FA + FS spherical beads. (b) UV–Vis DRS of TiO_2 and recycled composite.

iron oxides were also observed, confirming the dual nature of the catalyst even after recycling.

3.9. *Mineralization*

The mineralization study of isoproturon was carried out to determine the presence of anions such as nitrite and nitrate. There was reduction in COD during the treatment process, thereby verifying the increase in degradation as shown in Figure 11c. The reduction in TOC was also studied for confirming the mineralization of isoproturon (Figure S3). There is decrease in the concentration of nitrate ions for the duration of the experiment as there is a possibility of these ions being converted into nitrite ions. This is indicated by the effective increase in the concentration of nitrite ions as shown in Figure 11a,b,d. The relation between the degradation of isoproturon and the formation of various ions of nitrate, nitrite, and ammonium has also been studied (Figure S4).

The complete mineralization of the compound could be proved by GC–MS analysis for identification of the compounds formed during degradation. The proposed degradation mechanism (Figure 12) can follow two distinct routes of hydroxylation. Further fragmentation occurs by hydrodenitrogenation and yields 2-amino-5-isopropylbenzene-1,4-diol. The intermediate formed undergoes final fragmentation to produce acetaldehyde, 2-methyl butane, nitrate, nitrite, nitrogen, carbon dioxide, and water.

4. Conclusion

A hybrid concept of integrating an in situ dual effect of photo-Fenton and photocatalysis utilizing waste materials such as FS and FA has been successfully established for degradation of the compound isoproturon. The optimized conditions were specified using RSM based on BBD, which included H_2O_2 dose (700 mg·L^{-1}), number of composite beads (42)

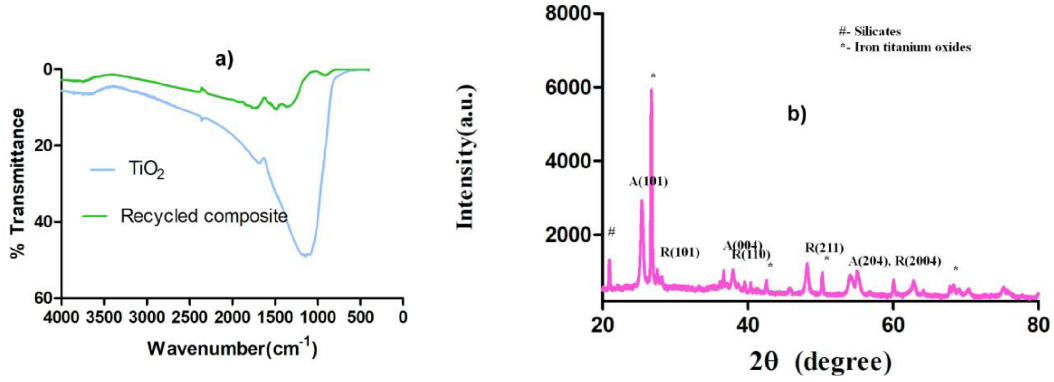

Figure 10. (a) FTIR of TiO_2, fresh composite. (b) UV–Vis DRS of TiO_2 and fresh composite.

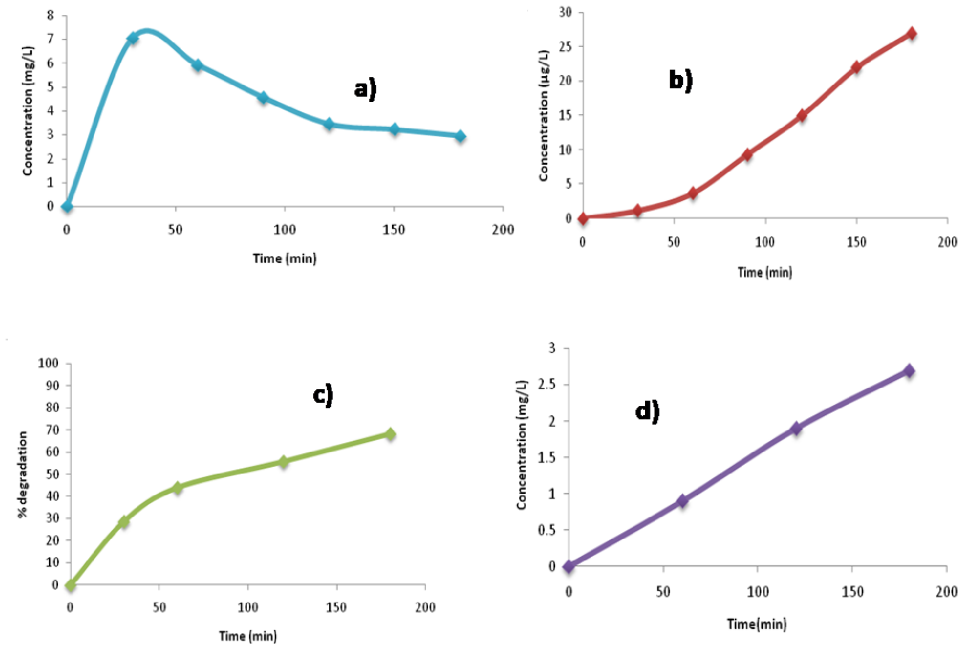

Figure 11. Mineralization analysis of isoproturon in terms of (a) nitrate, (b) nitrite, (c) COD reduction, and (d) ammonical nitrogen.

(i.e., covering 75% of the reactor's area), volume of wastewater (190 mL), and treatment time (176 min) showing degradation up to 80.96%. The integrated binary process followed pseudo-first-order kinetics, and overall 1.8 times synergy was obtained over the respective individual processes. Through the characterization of composite beads using SEM–EDS, UV–DRS, XRD, and FTIR, the presence of iron along with TiO_2 on the surface of beads was confirmed, hence proving the stability and utility of the integrated process. Mineralization of isoproturon by the production of nitrate, nitrite, and ammonia along with reduction in COD verified the degradation of the compound. The degradation mechanism was determined by identifying intermediates through GC–MS analysis. Hence, the integrated binary process using composite beads would provide a better alternative for treating wastewater containing pesticides.

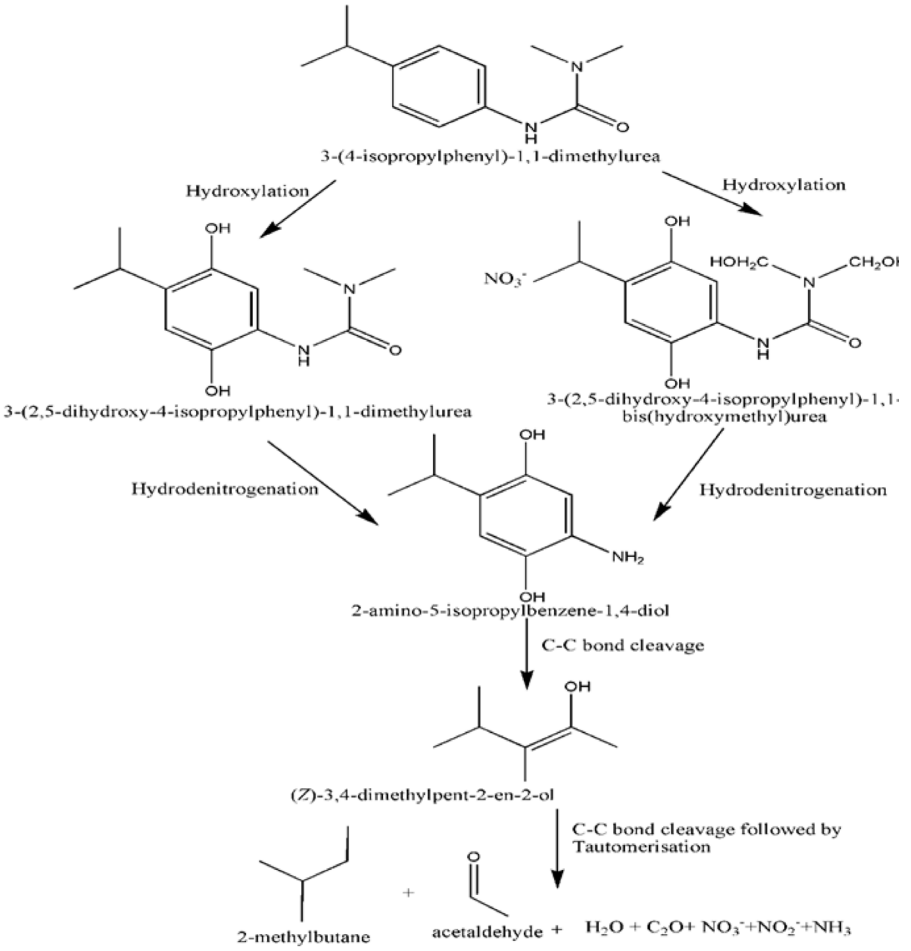

Figure 12. Proposed mechanism for degradation of isoproturon.

Data availability statement

All data, models, and code generated or used in the study appear in the published article.

Supplementary data

Supporting information for this article is available on the journal's website under https://doi.org/10.5802/crchim.52 or from the author.

References

[1] P. C. Abhilash, N. Singh, *J. Hazard. Mater.*, 2009, **165**, 1-12.
[2] P. B. Singh, V. Singh, *Environ. Toxicol. Pharmacol.*, 2008, **25**, 342-350.
[3] F. A. Ademola, A. I. Gideon, *Electron. J. Environ. Agric. Food Chem.*, 2012, **11**, 118-127.
[4] M. V. P. Sharma, V. D. Kumari, M. Subrahmanyam, *Chemosphere*, 2008, **72**, 644-651.
[5] P. R. Gogate, A. B. Pandit, *Adv. Environ. Res.*, 2004, **8**, 553-597.
[6] S. Devipriya, S. Yesodharan, *Sol. Energy Mater. Sol. Cells*, 2005, **86**, 309-348.
[7] A. D. Bokare, W. Choi, *J. Hazard. Mater.*, 2014, **275**, 121-135.
[8] A. N. Soon, B. H. Hameed, *Desalination*, 2011, **269**, 1-16.
[9] P. Bansal, A. Verma, *Chem. Eng. J.*, 2018, **332**, 682-694.
[10] A. C. Mecha, M. S. Onyango, A. Ochieng, C. J. S. Fourie, M. N. B. Momba, *J. Catal.*, 2016, **341**, 116-125.
[11] S. Talwar, A. K. Verma, V. K. Sangal, *J. Environ. Manage.*, 2019, **250**, article no. 109428.
[12] J. Yu, Q. Xiang, M. Zhou, *Appl. Catal. B Environ.*, 2009, **90**, 595-602.
[13] J. Ma, H. He, F. Liu, *Appl. Catal. B Environ.*, 2015, **179**, 21-28.
[14] L. Deng, S. Wang, D. Liu, B. Zhu, W. Huang, S. Wu, S. Zhang, *Catal. Lett.*, 2009, **129**, 513-518.
[15] P. Bansal, A. Verma, *J. Photochem. Photobiol. A Chem.*, 2017, **342**, 131-142.

[16] S. Talwar, V. K. Sangal, A. K. Verma, *Sep. Purif. Technol.*, 2019, **211**, 391-400.
[17] S. A. Kumar, G. S. S. Lekshmi, J. R. Banu, I. T. Yeom, *Water Qual. Res. J. Canada*, 2014, **49**, 223-233.
[18] APHA/WEF/AWWA, "4500-NO2 NITROGEN (NITRITE) (2017)", in *Standard Methods For the Examination of Water and Wastewater (2018)*.
[19] APHA/AWWA/WEF, "500 - Nitrate - Ultraviolet Spectrophotometric Screening Method", in *Standard Methods For the Examination of Water and Wastewater (2005)*.
[20] APHA/AWWA/WEF, "4500-NH3 Nitrogen (Ammonia)", in *Standard Methods For the Examination of Water and Wastewater (2005)*.
[21] APHA, "500-Fe B Phenanthroline Method", in *Standard Methods For the Examination of Water and Wastewater (2017)*.
[22] APHA, "4500-NO2 NITROGEN (NITRITE) (2017)", in *Standard Methods For the Examination of Water and Wastewater (2018)*.
[23] A. Aleboyeh, Y. Moussa, H. Aleboyeh, *Dye. Pigment*, 2005, **66**, 129-134.
[24] V. K. Pareek, M. P. Brungs, A. A. Adesina, R. Sharma, *J. Photochem. Photobiol. A Chem.*, 2002, **149**, 139-146.
[25] S. S. Lin, M. D. Gurol, *Environ. Sci. Technol.*, 1998, **32**, 1417-1432.
[26] S. Talwar, V. K. Sangal, A. Verma, *J. Photochem. Photobiol. A Chem.*, 2018, **353**, 263-270.
[27] P. Bansal, A. Verma, S. Talwar, *Chem. Eng. J.*, 2018, **349**, 838-848.
[28] M. Dietrich, M. Franke, M. Stelter, P. Braeutigam, *Ultrason. Sonochem.*, 2017, **55**, 165-176.